Chemical Engineering Journal 481 (2024) 148454

Contents lists available at ScienceDirect

Chemical Engineering Journal

journal homepage: www.elsevier.com/locate/cej

Polyaniline/activated carbon composite based flowing electrodes for highly efficient water desalination with single-cycle operational mode

Kunyue Luo [a], Tong Hu [b], Wenle Xing [c], Guangming Zeng [a,*], Wangwang Tang [a,*]

[a] College of Environmental Science and Engineering and Key Laboratory of Environmental Biology and Pollution Control (Ministry of Education), Hunan University, Changsha 410082, China
[b] Department of Environmental Science, Zhejiang University, Hangzhou Zhejiang 310058, China
[c] School of Resources and Environment, Hunan University of Technology and Business, Changsha 410205, China

ARTICLE INFO

Keywords:
Capacitive deionization
Water desalination
Polyaniline-activated carbon composite

ABSTRACT

Flow-electrode capacitive deionization (FCDI) is a promising technique for water desalination and has received considerable attention. The desalination efficiency of FCDI is significantly influenced by the flowing electrode material. Therefore, it is necessary to develop highly efficient flowing electrode materials to obtain excellent desalination capability. Polyaniline (PANI) is regarded as a promising pseudocapacitive material with high conductivity and desirable hydrophilicity. Herein, in order to improve the stability of PANI, a rod-like polyaniline loaded on activated carbon (AC) was prepared by a simple in-situ polymerization to obtain the PAC composite for FCDI electrode. The composite successfully combined the characteristics of AC and polyaniline. The desalination performance of PAC composite for FCDI single-cycle mode was explored, and the mechanism was ascribed to the synergy between electric-double layer capacitance of AC and pseudocapacitance of PANI. The PAC-9 composite with the best electrochemical performance achieved a salt removal efficiency of 94.3 % and an average salt removal rate of 0.963 μmol cm^{-2} min^{-1} at 1.2 V. In addition, the PAC-9 composite did not decay after 12 h of long-term operation, showing that the composite is a promising active material for water desalination.

1. Introduction

Freshwater is an important resource that is indispensable to human survival and development. Nevertheless, with the rapid growth of population and industrialization, the water scarcity has become a crisis that the world must face together. How to provide sufficient clean water is the key concern of human beings at present and even for a long time in the future [1–4]. The development of new and advanced desalination technologies to utilize the abundant salty seawater resources to solve the water scarcity problem has become one of the most attractive strategies [5–7]. Although several conventional desalination technologies such as distillation and membrane separation desalination technologies have been widely utilized, these technologies have disadvantages such as high energy consumption, large operating costs, and potential secondary pollution, which do not match the demand for sustainable development [8–12].

Capacitive deionization (CDI) is an emerging energy-efficient and environmentally friendly water desalination technology in which ions are adsorbed on or within the electrodes through electrostatic interactions or Faradaic redox reactions [13–17]. However, the desalination capacity and intermittent salt removal by CDI static electrodes make their applications limited. To overcome the limitation of fixed electrode, the flow-electrode capacitive deionization (FCDI) was developed with the use of flowable electrode [18–21]. Although the FCDI technology improves the desalination performance of the conventional CDI technology with obvious advantages and potential, the conductive electrical network of the suspended active material (usually activated carbon) in the flow-electrode slurry is discontinuous, leading to the conductivity of the flow-electrode slurry being several orders of magnitude smaller than the traditional fixed electrode, which affects the charge transfer and limits the desalination efficiency to some extent [22–24]. The collision between electrode particles can be increased by improving the mass percentage of active materials in the flowing electrode, which can enhance charge transport and desalination performance [25–28]. Nevertheless, FCDI systems are expected to be flowable, and higher solid content can lead to increased viscosity, causing the risk of channel

* Corresponding authors.
E-mail addresses: zgming@hnu.edu.cn (G. Zeng), wtang@hnu.edu.cn (W. Tang).

https://doi.org/10.1016/j.cej.2023.148454
Received 22 October 2023; Received in revised form 22 December 2023; Accepted 28 December 2023
Available online 2 January 2024

clogging. Currently, an active material content of about 5–10 wt% is a generally stable and practical operation content to ensure the flowability of slurry electrodes [27–30]. To enhance the desalination efficiency of FCDI systems, it is an important measure to improve the electrochemical properties of AC suspension at a certain slurry solid content.

From the perspective of electrode materials, in addition to carbon-based electrodes that rely on an electric-double-layer capacitance (EDLC) storage mechanism, Faradaic pseudocapacitive materials based on reversible redox types can also lead to high capacitance, and have been extensively researched in recent years [31–36]. Thus, alternative methods to improve the performance of the suspension electrode could be combining pseudocapacitive materials with EDLC materials [37–42]. Conductive polymers are an attractive type of pseudocapacitive materials [43–45]. Among them, polyaniline (PANI) as one of the most widely used conductive polymers, is considered to be a highly promising pseudocapacitive material with the advantages of high electrical conductivity, excellent reversible redox, large theoretical capacitance, desirable hydrophilicity, and easy synthesis, etc. It has received a lot of attention from researchers. The PANI has three ideal states: pernigraniline, emeraldine, leucoemeraldine [44–48]. However, PANI is prone to expansion and shrinkage during charging and discharging, which leads to structural dissociation and affects its long-term cycling stability. It has been suggested that the combination of porous carbon, graphene, carbon nanotubes and other carbon-based materials with PANI can improve the electrode ability and cycling stability [49,50].

In this study, in order to overcome the drawbacks and fully utilize the advantages of polyaniline, polyaniline was selected to be loaded on activated carbon (AC) by in-situ polymerization growth, using the pores of AC as the capture and retention sites of polyaniline to construct rod-like PAC composite. It can benefit from both the high specific surface area of AC and the pseudocapacitance of PANI due to the fast surface or near-surface redox reactions. By verifying the property that PANI contains both oxidized and reduced state, the desalting performance of PAC composite in the FCDI unit was investigated in SC mode, and the associated mechanism was also explored. Finally, the stability of PAC composite was examined through long-term cycling experiment.

2. Materials and methods

2.1. Synthesis of PAC composite

The PAC composite was synthesized by in-situ chemical polymerization of aniline monomers in AC via the use of ammonium persulfate (APS) as the oxidant in the acidic medium (HCl). During polymerization, 3, 5, 7, 9, 11 and 13 g of AC were added to synthesize PAC composite with different polyaniline loading, and the composite samples were denoted as PAC-3, PAC-5, PAC-7, PAC-9, PAC-11 and PAC-13, respectively. Briefly, 0.1 M of APS was dissolved in 100 mL of ultrapure water with stirring lasting 30 min and subsequently placed in the refrigerator to cool for use. In another beaker, 0.1 M aniline monomer (n (APS):n (aniline) = 1:1) was mixed with 100 mL of 1 M HCl solution with stirring lasting 30 min. Afterwards, AC (3, 5, 7, 9, 11, 13 g) was dispersed into the prepared solution with stirring lasting 1 h, so that the aniline monomer was immersed in the activated carbon slurry. The cooled APS solution was added drop by drop to the aniline monomer-soaked activated carbon dispersion system to induce the polymerization, and then kept stirring for 24 h. It is worth noting that the entire synthesis experimental process had been surrounded by ice cubes, and stirred by employing a magnetic stirrer. Then, ethanol and deionized water were used to wash the PAC composite to remove the unstable polyaniline. Finally, the PAC composites with different polyaniline loadings were dried in an oven at 60℃. The control activated carbon obtained according to the above PAC composite synthesis method without the addition of aniline was marked as “Blank”.

2.2. FCDI operation and performance evaluation

A detailed description of the FCDI unit was presented in the Supporting Information. It was a typical three-chamber FCDI unit made up of acrylic end plates, graphite plates with snake-like channels (3 mm wide, 3 mm deep, and 819 mm long) and ion exchange membrane, as displayed in Figure S1. The effective contact area between the flowing electrodes and the ion exchange membrane was ~ 24.6 cm^2. The schematic diagrams of the isolated closed-cycle (ICC) and single-cycle (SC) modes are shown in Figure S2. Except for the long-term experiment, the feed water was 50 mL of 2 g L^{-1} NaCl solution, which flowed into the middle chamber through a peristaltic pump at 25 mL min^{-1} and was recycled. The effluent conductivity was measured via a conductivity meter during all the experiments. The constant voltage to the FCDI cell was applied through a direct-current power supply. The current probe (DCP-BTA) was connected with the data acquisition system (Sensor DAQ, Vernier, America) to monitor the current charges during the desalination process. The flowing electrode operated in SC mode was prepared by dispersing 10 % active material (AC Blank or PAC composite) and 2 % carbon black into 200 mL of 2000 mg L^{-1} NaCl aqueous solution. The flow-electrode slurry is pumped into the anode with a flowrate of 50 mL min^{-1} and flows directly from the anode outlet to the cathode chamber, and finally returns to the reservoir. For the ICC mode, the anode and cathode flowing electrodes were composed of 100 mL of 2000 mg L^{-1} NaCl, 5 wt% of active substance and 1 wt% of carbon black, respectively.

The detailed information about the used chemicals in this study, the material characterization method, the electrochemical characterization method, and the performance indicator calculation methods can be found in the Supporting Information.

3. Results and discussion

3.1. Characterization of the prepared materials

As shown in Fig. 1, morphologies of AC, PANI and PAC composite were investigated via SEM characterization. The Fig. 1d–f clearly shows that the pure PANI monomer exhibits nanorod-like morphological agglomerates. Apparently, the PAC composite is well covered by PANI due to the in-situ polymeric growth of the nanorod-like structured PANI on the AC surface (Fig. 1g–i), which results in a rougher surface of the PAC composite compared to the pristine AC particles that appear to have a smooth surface with abundant micropores (Fig. 1a–c). Figure i shows the microscopic morphology of the PAC composite, where PANI is attached to the AC surface pores and the adjacent rods gradually grow together to form a three-dimensional (3D) interconnected network architecture that is cross-linked to each other. The pores of AC act as a capture and retention site for conductive PANI, which can prevent its degradation and improve its stability. At the same time, in addition to providing electrochemically active sites for fast Faradaic redox reactions, the rod-like structure facilitates enough contact between the electrolyte and the electrode, which is conducive to the rapid migration of electrolytes and access to the interior of the electrode material. Therefore, the 3D porous cross-linked loading of the conducting PANI as a bridge for charge transfer between adjacent layers can induce a large number of defects on the AC, which facilitates the generation of more accessible surface sites and improves the electron transfer efficiency.

Conductive PANI polymerization on the surface of AC particles may change the specific surface area (SSA) and pore structure, and hence the structure characteristics of the material were determined by the N_2 adsorption and desorption method, and the results were displayed in Figure S4 and Table S3. As shown in Figure S4a, the isotherms of the blank are typical type I isotherm features based on the IUAC classification, and the rapidly increasing N_2 at low pressure indicates the dominance of microporous structures. All the PAC composites exhibit a typical type IV isotherm property with the presence of a hysteresis loop,

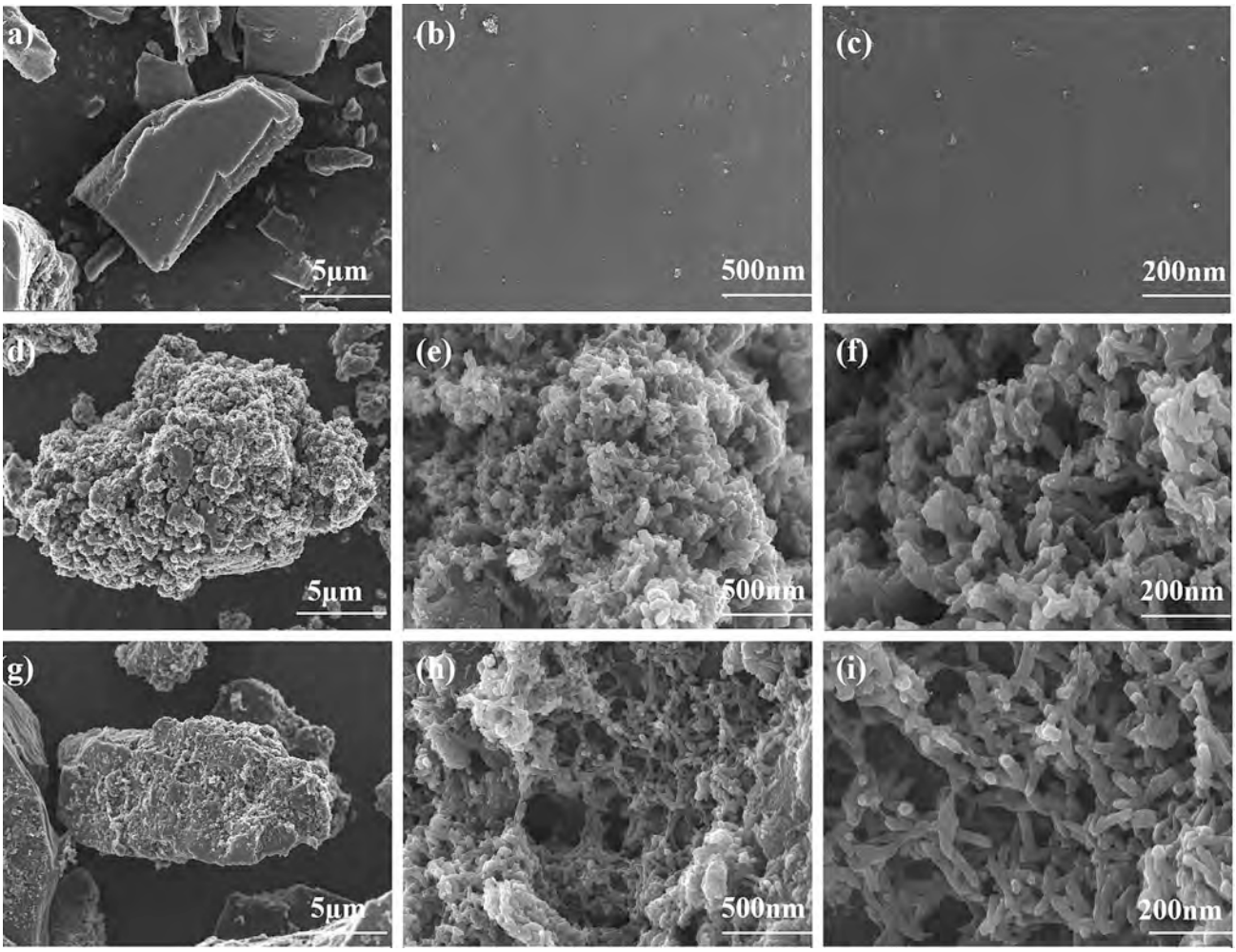

Fig. 1. SEM images of (a-c) AC,(d-f) PANI, (g-i) PAC composite in different magnifications.

implying the presence of mesopores. The pore size distribution of the blank and PAC composite is shown in Figure S4b, which also demonstrated the existence of microporous and mesoporous structures, and suggested that the PAC composite was more mesoporous. The abundant pore structure of the PAC composite can provide plentiful adsorption sites and shorten the diffusion channels. From Figure S4a and Table S3, it could be observed that the surface area and pore volume of PAC composite were significantly reduced compared to the blank, which could be caused by the change in the effectiveness of the surface loading of the conductive PANI. This means that the conductive PANI loading causes the micropores on the AC surface to be filled and the number of micropores to decrease, resulting in a reduction in SSA and an increasing average pore size. The reduction of micropores in PAC composite may reduce the adsorption performance, whereas the mesopores facilitate ion transport/diffusion, and thus the PAC composite with a hierarchical pore structure possibly leads to a better electrosorption performance and enhanced desalination efficiency of the FCDI.

The crystal structures of AC, PANI and PAC composite were analyzed through XRD patterns in Figure S5. The pristine AC shows two broad diffraction peaks at 23.5° and 43.2° which is in line with the (0 0 2) and (1 0 1) crystal planes, respectively, and indicates that it is an amorphous carbon material. The PAC composite overlapped with the typical peaks of PANI, with diffraction peaks at 14.9°, 20.1° and 25.2° ascribed to the diffraction crystallographic planes (0 1 1), (0 2 0) and (2 0 0) of PANI [51–54]. The PAC composite mainly show peaks at $2\theta = 25.2°$, which is related to the formation of the amorphous PANI. The intensity of the diffraction peak at 43.2° is not evident for the activated carbon after the in-situ polymerization growth of PANI on the AC surface, which also confirms the successful loading of PANI on the AC surface and pores as well as the reduced graphitization of the composite.

The FTIR spectra of pristine AC, blank, PANI, PAC-9 and the PAC after the long-term experiment (LPAC-9) are displayed in Fig. 2a. For the AC spectrum, the peaks at approximately 3431 cm^{-1}, 2923 cm^{-1}, 1609 cm^{-1} and 1189 cm^{-1} are ascribed to the O-H stretching vibration, the C = C bond, the $–CH_2$ symmetric stretching and the C-O stretching vibration, respectively. A typical group of peaks corresponding to PANI appears in the spectrum of PAC composite compared to AC. The peak at 3431 cm^{-1} belongs to the N-H stretching vibrations of PANI. Furthermore, the quinone structure has a characteristic stretching vibration peak of N = Q = N (Q is the quinone ring) at 1565 cm^{-1} and the benzene ring has a stretching vibration absorption peak of C = C at 1446 cm^{-1} with similar peak intensities. Moreover, the peaks at 1298 and 1247 cm^{-1} are related to the C-N stretching vibrations, and the peak at 1100 cm^{-1} is related to the imine nitrogen -B-N = Q- structure (B is the benzene ring) [51,53,55,56]. The characteristic absorption peak at 795 cm^{-1} can be due to the out-of-plane bending vibration of C-H for the benzene ring. It is obvious that the spectra of all the composite showed characteristic peaks of PANI and AC, confirming the successful loading of PANI on the AC surface. In the meantime, according to the above results, the PANI loaded on the AC can be regarded as a highly conductive emeraldine. It means that the PAC composite can be in both oxidized state and reduced state in the electrochemical process to obtain high pseudocapacitance. In addition, the characteristic peaks of PAC composite shifted slightly and the peak intensity got weakened

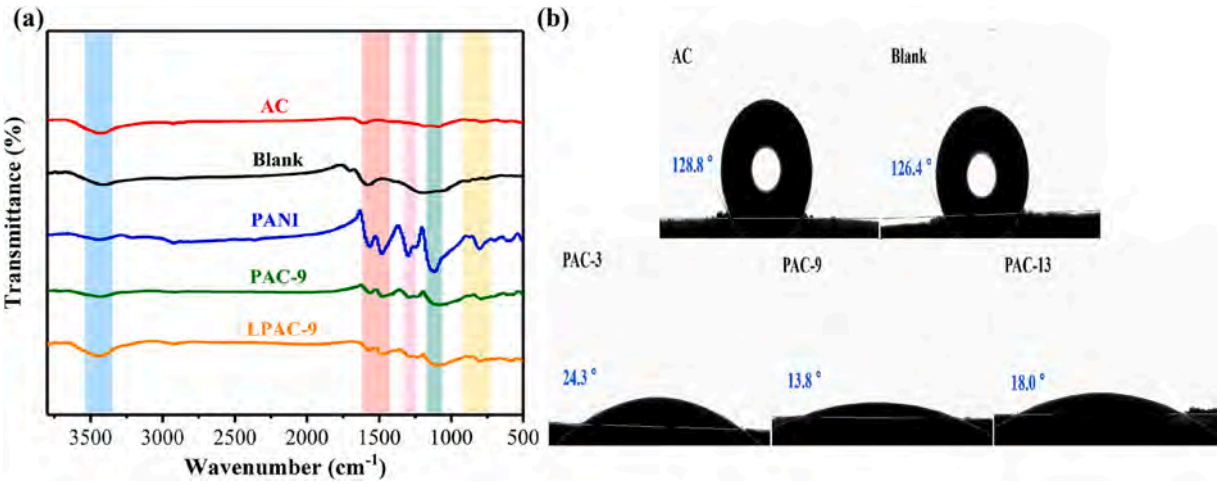

Fig. 2. (a) FTIR spectra of pristine AC, Blank, PANI, PAC-9 and the PAC after the long-term experiment (LPAC-9); (b) Water contact angles of pristine AC, Blank, PAC-3, PAC-9, PAC-13.

compared to PANI, which also indicates the successful loading of PANI. The electron delocalization degree of PANI monomer is lower, thus resulting in the electron transition of PAC composite being easier, which is expected to improve the electrochemical performance of the material and enhance the desalination efficiency.

The high wettability of electrode materials is expected to enhance the desalination efficiency of FCDI. In order to determine the wettability of PAC composite, a water contact angle measurement was performed. The results are shown in the Fig. 2b. The water contact angle measurement confirmed that the in-situ polymerization of polyaniline on the surface of AC significantly improved the hydrophilicity of the PAC composite electrode material, and with the increase of activated carbon addition, the contact angle of PAC composite first decreased sharply and then increased slightly, in which PAC-9 had the strongest hydrophilicity. The contact angle of PAC-9 is reduced from 128.8° to 13.8° compared with the AC Blank. The conductive PANI transforms the hydrophobic

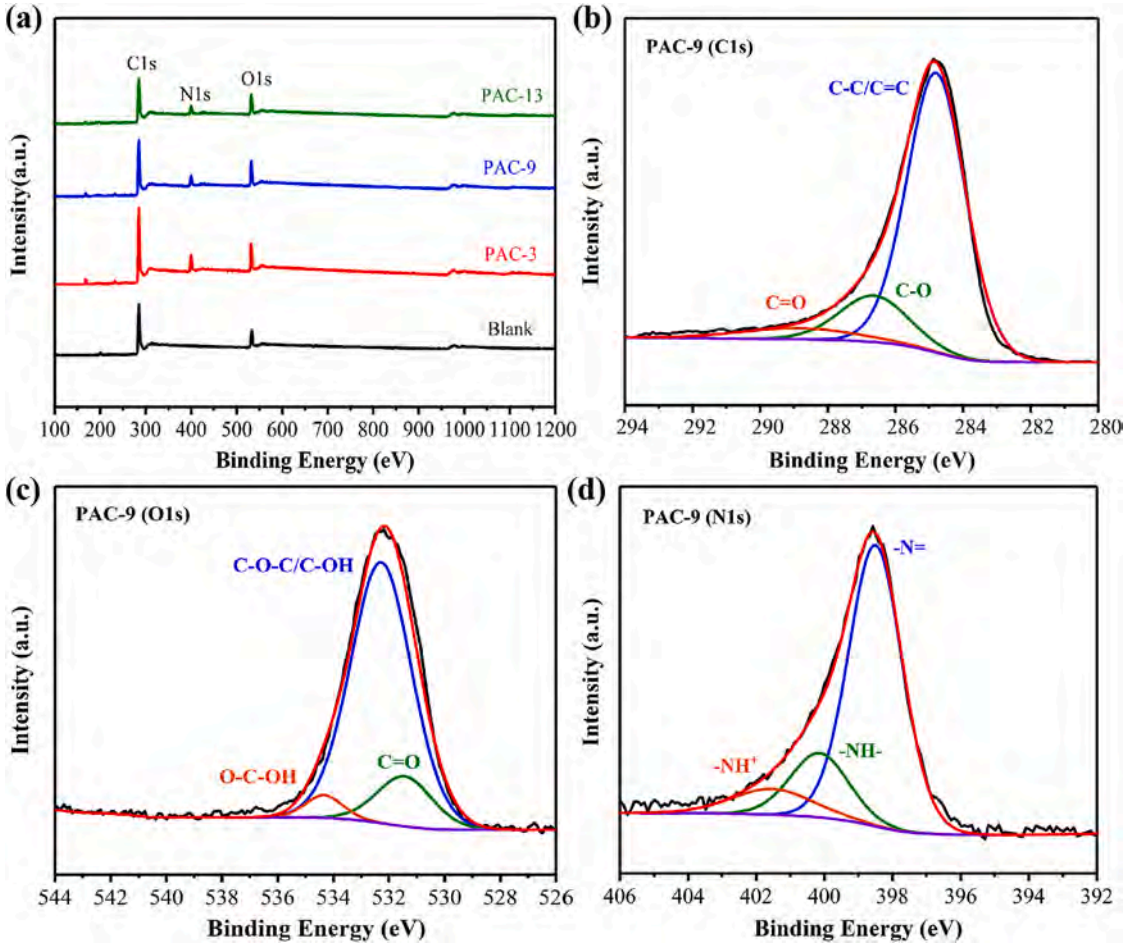

Fig. 3. (a) XPS survey spectrum of Blank, PAC-3, PAC-9 and PAC-13; High-resolution (b) C1s spectrum, (c) O1s spectrum and (d) N1s spectrum of PAC-9 composite.

carbon surface into hydrophilic, which can greatly enhance the ion capture on the surface of the electrode material during FCDI desalination process, and facilitate the rapid transfer of electrolyte ions and improve the desalination efficiency. This would be subsequently confirmed.

XPS spectra were adopted to examine the surface element composition and chemical bond structure of the synthetic materials. The characterization results of AC, Blank and PAC composite are shown in the Fig. 3a, which clearly shows the composition changes of the materials. The peaks of C1s (284.8 eV) and O1s (532.8 eV) were observed in all the samples [55,57]. An additional peak of N1s (400.0 eV) is present in the spectra of different PAC composites [54,58]. To obtain more information about the chemical structure, the C1s, O1 sand N1s curves of the PAC-9 composites were deconvolved (Fig. 3b–d), while the results

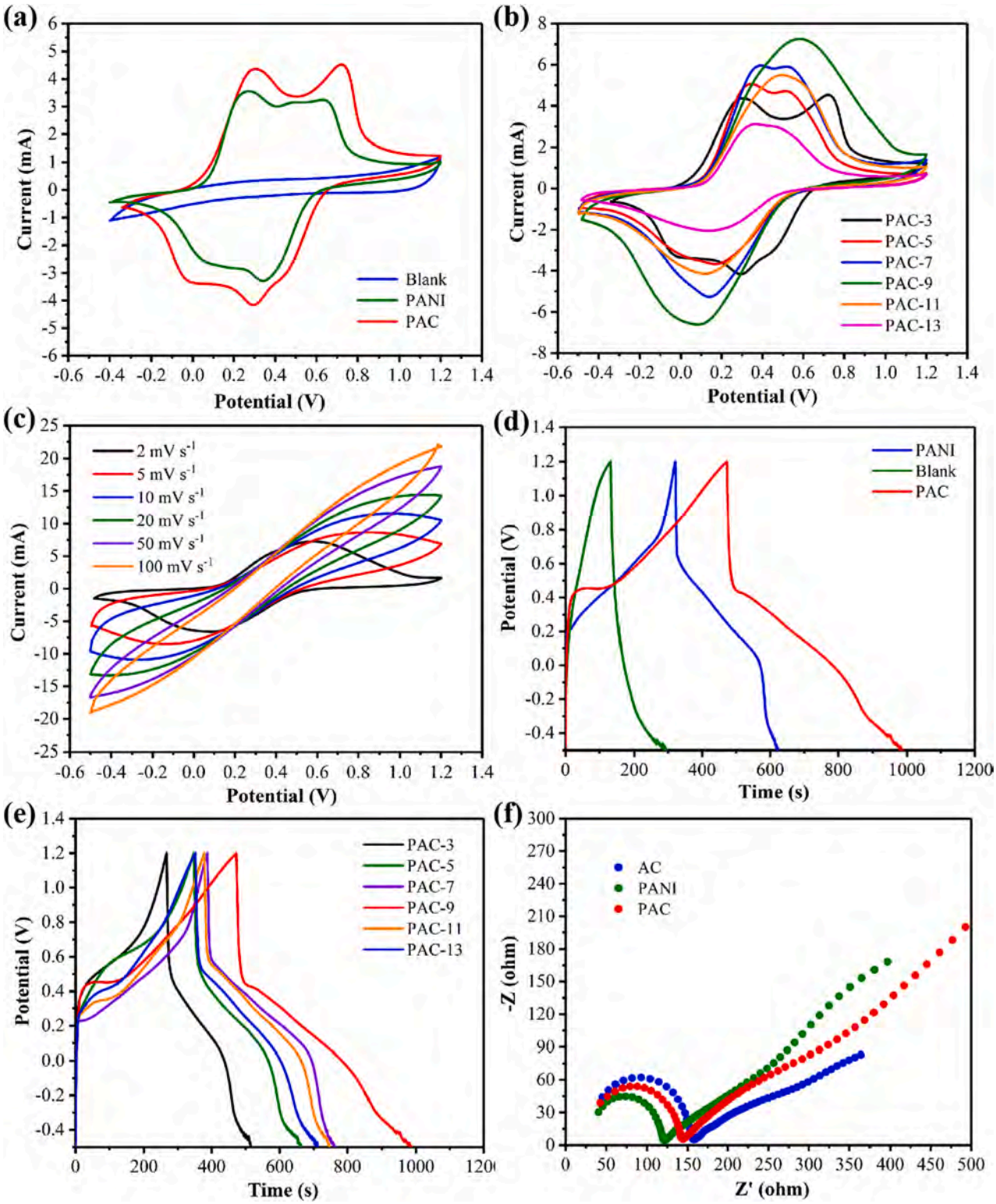

Fig. 4. CV results of the (a-b) various electrodes at 2 mV s^{-1}, and (c) PAC-9 at varying sweep rates (2, 5, 10, 20, 50 and 100 mV s^{-1}); (d-e) the GCD curves of the various electrodes at 0.01 A/g; (f) Nyquist plots of the electrodes.

were compared with the pristine AC (Figure S6).

The high-resolution C1s deconvolution mapping of the pristine AC and PAC composite shows a significant peak at 284.8 eV, indicating the presence of graphitic carbon. Notably, the C1s peak of the pristine AC in the broad spectrum is stronger than that of the PAC composite, which demonstrates that the loading of PANI successfully reduces the graphitic carbon content of the PAC composite and supports the XRD analysis. The high-resolution C1s spectra of PAC-9 composite show three peaks at 284.8, 286.6 and 288.57 eV, which belong to the C-C/C = C, C-O and C = O structures, respectively (Fig. 3b), and match well with the C1s peak of AC (Figure S7a) [54,59,60]. The Fig. 3c shows the deconvoluted O1s spectra of PAC-9 composite, which suggests the existence of quinone (C = O, 531.4 eV), hydroxyl (C-O-C or C-OH, 532.2 eV) and carboxylic (O-C-OH, 534.4 eV) groups [61,62]. In the Fig. 3d, the high-resolution spectrum of N1s for PAC-9 composite can be deconvoluted into three characteristic peaks, corresponding to the quinonoid imine structure (-N =) at 398.5 eV, benzenoid amine structure (–NH-) at 400.5 eV and nitrogen cationic radical structure ($–NH^+$) at 401.3 eV [63–67]. These peaks prove the success of PANI loading on AC. The same results were obtained for PAC-3 and PAC-13 composites by deconvolution of different elemental curves (Figure S6). Moreover, the XPS full scan spectra showed that the intensity of the N1s peak of the PAC composite gradually decreased with the increase of the activated carbon content, indicating that the load of polyaniline decreased. As for the –NH group in the N1s peak, it not only can generate the pseudocapacitance by the loss of electrons to form C = N, but also can increase hydrophilicity, which is conducive to the transfer of ions from the electrolyte solution to electrode material. It is noteworthy that the presence of the -N = and $–NH^+$ groups in the PAC composite also facilitates the enhancement of the electron conductivity, reducing the internal resistance of the electrode and improving the capacitance. In summary, on the one hand, the different N functional groups of the PAC composite can enhance electron transfer and capacitance by improving the conductivity of electrode materials. On the other hand, the PAC composite can obtain additional capacitance via Faradaic redox reactions apart from electric-double-layer capacitance. This would be also verified in the subsequent electrochemical results.

3.2. Electrochemical tests

To investigate the mechanism of the PAC composite as flowing electrodes to improve the desalination efficiency of FCDI, the electrochemical characteristics of the electrodes were investigated via cyclic voltammetry (CV), electrochemical impedance spectroscopy (EIS) and galvanostatic charging-discharging (GCD). Fig. 4a presents the CV results of AC Blank, PANI monomers and PAC-9 composite at a scanning rate of 2 mV s^{-1}. The curve of the AC Blank is an approximately symmetrical rectangle, indicating that it has a typical electrochemical electric-double-layer capacitance. The CV curves of PANI monomer and PAC composite deviate from the ideal rectangle and a pairs of redox peaks can be observed implying that the pseudocapacitive was provided, which can be ascribed to the reversible faradaic reactions between the leucoemeraldine/emeraldine and emeraldine/pernigraniline of PANI [66,68]. The enclosed area of the CV profile is often used to evaluate the specific capacitance of an electrode. Obviously, the enclosed area of the CV profile of the PAC composite is significantly enhanced compared to the blank electrode, indicating that PANI contributes significantly to the total capacitance of the PAC composite through a reversible faraday redox reaction. It is noteworthy that the specific capacitance of the composite electrodes got enlarged with the addition of AC from 3 to 9 g, but decreased at higher AC content (Fig. 4b and Table S4). The above trend proves that an excessive AC content could lead to an insufficient charge transfer utilization of PANI in the 3D interconnected structure and a decrease of Faradaic redox reaction, thus reducing the specific capacitance of the PAC composite. It can be seen that appropriate AC content is very important for the optimal electrochemical performance of PAC composite. The specific capacitance of different PAC composites is shown in the Table S4. Among them, the maximum capacitance of PAC-9 composite is 335.94F g^{-1}, which is 6.7 and 1.8 times that of the blank electrode and PANI monomers, respectively. The cyclic voltammetry of PAC-9 composite at different scan rates was investigated with the results shown in Fig. 4c. In the range of 2–100 mV s^{-1}, the CV curve shape of PAC-9 composite did not change with increasing scan rate, reflecting that the electrode material has a good reversibility.

The electrochemical properties of PAC composite under controlled current conditions were analyzed by galvanostatic charging-discharging. As shown in the Fig. 4d, the GCD curve of the blank electrode is approximately a symmetric triangle, indicating that it has ideal EDLC characteristics. However, the GCD curve of PANI and PAC composite have a linear deviation from the ideal triangular shape with humps, which presented typical pseudocapacitance characteristics, indicating that the capacitance of the electrode materials mainly came from the electric double-layer capacitance of AC and the pseudocapacitance of the PANI. Meanwhile, the PAC composites apparently have longer charge–discharge time than the blank electrode and correspondingly have better specific capacitance values, which demonstrated that the loading of PANI on AC is conducive to enhancing the charge storage and ion adsorption capacity of the electrodes. There was no significant IR drop observed in the GCD curves of all the PAC composites (Fig. 4e), which indicates that the composites have low internal resistance. In addition, as shown in Figure S8a, the GCD curves of PAC-9 composite remained unchanged at high current densities, which implies that the composite has high electrochemical reversibility and fast charge–discharge performance. It is worth noting that the changing trend of specific capacitance for the PAC composites with different PANI loading ratios is similar to that of CV curve, which also confirms that PAC-9 has the optimal specific capacitance value at a specified current density.

The charge transfer capability and ion diffusion properties of the PAC composites were characterized by electrochemical impedance spectra (EIS). As displayed in Fig. 4f and S8b, all the samples exhibit similar Nyquist curves with a quasi-semicircles and a diagonal in the high-frequency region and low-frequency region, respectively. The diameter of the quasi-semicircles in the high-frequency region indicates the charge transfer resistance (R_{cts}) between the electrode material and the electrolyte solution interface, and the larger quasi-semicircles implies the greater R_{cts}. The slope of the diagonal in the low-frequency region represents the Warburg impedance (Z_w) due to the ion diffusion from the electrolyte to the electrode, and the larger slope indicates smaller diffusion resistance and quicker ion transfer for the electrode. According to the Nyquist plots, the semicircle diameter of the PANI and PAC composite were smaller than the pristine AC, demonstrating smaller interfacial charge transfer resistance to enable fast charge–discharge rates, which can be attributed to the sufficient wettability and high electrical conductivity due to the in-situ growth of PANI. These results suggest that appropriate PANI loading was beneficial to reduce the ion transport resistance at the interface between the PAC composite electrode and the electrolyte to improve the conductivity of the electrode and obtain an ideal ion diffusion ability. The Figure S8b shows that all the PAC composites have a slant line of about 45° in the low-frequency range, which is characteristic of pseudocapacitance and implies fast ion diffusion and adsorption behavior. It can be attributed to the coupling interaction of PANI with AC as a result of the 3D interconnected mesoporous structure constructed by the rod-like structured PANI acting as a charge transfer bridge and fast diffusion channel.

The above results demonstrate that, among the prepared samples, PAC-9 composite can achieve efficient utilization of electrode components with the best electrochemical performance and has the opportunity to result in excellent water desalination performance. This would be validated in the following desalination experiments.

3.3. Desalination performance

Among the several operational modes of FCDI, the single-cycle (SC) mode exhibits a single closed flow loop path with the flowing electrode circulated in the anodic and cathodic chambers [69]. Desorption and adsorption occur simultaneously when the flowing electrode in one chamber enters directly into the other chamber, and thus the SC mode operates without the need for separate discharging process. Compared to the sequential adsorption and desorption in the isolated closed-cycle (ICC) mode, the timely desorption in SC mode helps to renew the active material throughout the desalination process and has more available electrosorption capacity, which results in better desalination performance. It is worth noting that simultaneous charging and discharging in SC mode also makes efficient use of electrostatic energy in the desorption process, thus reducing energy consumption. Therefore, considering the characteristics that PAC composites have oxidation unit and reduction unit at the same time, a desalination experiment was conducted in SC mode to evaluate the desalination efficiency of the PAC composite and to investigate the associated mechanism.

Firstly, the effectiveness of PAC composite consisting of oxidation units and reduction units was verified by comparing the salt removal efficiency of PAC composite acting as anode/cathode only for ICC mode at a constant voltage of 1.2 V. Figure S9 shows the variation in the conductivity of the effluent with time during the FCDI operation. In the ICC mode, no significant difference in the effluent conductivity was found for the blank flowing electrode only acting as anode or cathode, and both of them showed salt removal efficiencies of around 24 %, which was lower than PAC (anode) and PAC (cathode). In particular, PAC (cathode) exhibited the best desalination performance with a salt removal efficiency of 52 %, which was slightly higher than that of PAC (anode) at 42 %. It may be due to the higher proportion of oxidation units loaded in PAC composite. According to the N1s curve of XPS, it can be confirmed that the percentage of oxidation units is significantly higher than that of reduction units, and the intensity of the oxidation peak of the CV curve is slightly higher than that of the reduction peak, which indicates that more redox reactions occur during the reduction process of PAC composite, thus providing a larger pseudocapacitance. The above results demonstrate the potential of PAC composite to be used in SC mode to achieve energy saving and excellent desalination efficiency via both oxidation reaction at the anode and reduction reaction at the cathode, which can effectively improve the desalination efficiency.

The desalination performance of PAC composite operated in SC mode was investigated via the calculation of salt removal efficiency (SRE) and average salt removal rate (ASRR). As shown in Fig. 5, the SRE of the blank as the flowing electrode was 22.7 % and 41.6 % after 30 min and 60 min of operation, respectively. In contrast, the SRE of the PAC-9 composite acting as the flowing electrode increased significantly to 75 % at 30 min, which was 3.3 times higher than that of the blank electrode, and 94.3 % at 60 min. Moreover, the average salt removal rate with PAC-9 composite was 0.963 μmol cm^{-2} min^{-1}, and the charge efficiency was elevated from 53 % to 79 %, while the energy consumption was as low as 8.21 μmol J^{-1}, indicative of the relatively good desalination performance of the PAC composite when compared with other materials-based FCDI electrodes (Table S6).

Based on the above results, the effects of PAC composites with different PANI loadings on the desalination performance in SC mode were investigated. As shown in Fig. 5b, the variation of effluent conductivity for PAC composites with different PANI loadings was in accordance with the results of electrochemical analysis, and in addition, their desalination performance was better than the blank flowing electrode. The PAC-9 composite had the best desalination performance, including enhanced desalination capacity, faster SRE and higher CE. It can be attributed to the rod-like PANI layer constructing a highly conductive 3D interconnected network architecture, which facilitates improved ion diffusion/transfer performance. Crucially, the PANI acts as a fast faraday redox active site to provide pseudocapacitance. As a result, a synergistic mechanism of electric-double-layer and pseudocapacitance deionization is proposed for the PAC composite based on the

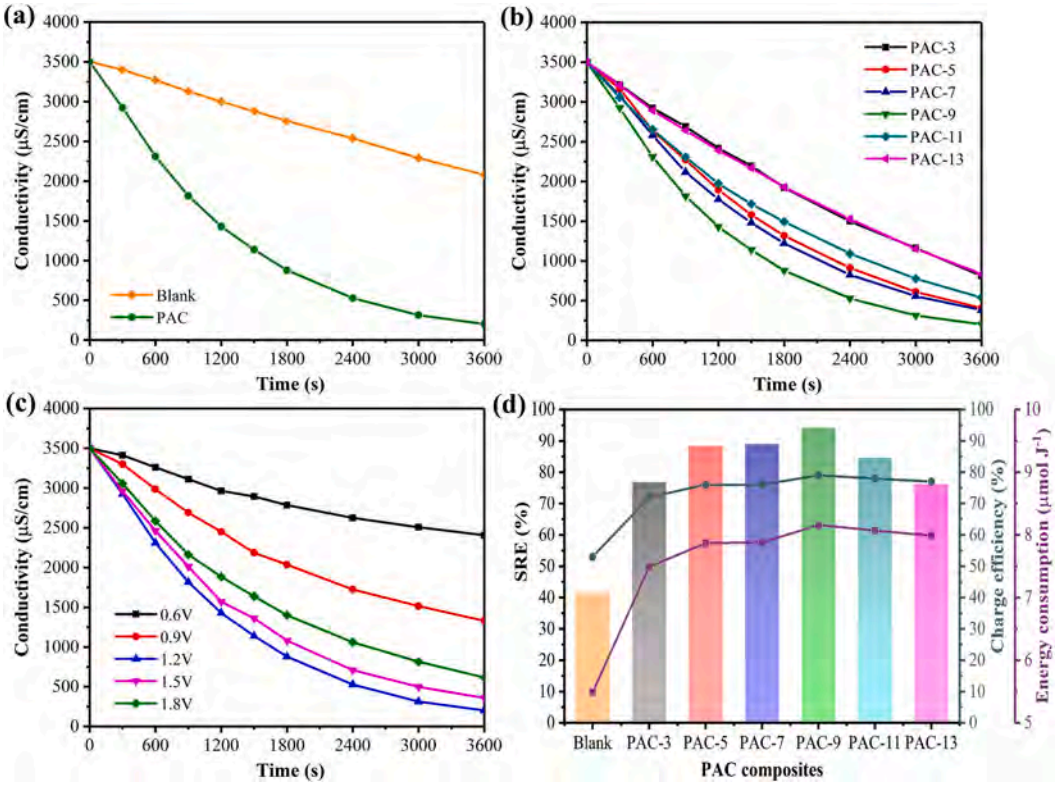

Fig. 5. Temporal variation of effluent conductivity with (a) Blank and PAC composite flowing electrodes under SC operation mode, (b) the PAC composites with different PANI loadings, (c) different applied voltages; (d) Variations in the SRE, CE and ENRS by using different electrodes.

electrochemical characterization analysis as well as the desalination results, that is, both the Faradaic pseudocapacitance of PANI coupled with the electric-double-layer capacitance of AC played a crucial role in enhancing the desalination performance of FCDI. The mechanism of the redox reaction of PANI was displayed in the Fig. 6.

Finally, with the aim of investigating the influence of charging voltage on the performance of PAC composite for FCDI, different voltages (0.6, 0.9, 1.2, 1.5, 1.8 V) were applied with PAC-9 composite as the flowing electrode. As can be seen from Fig. 5c, the effluent conductivity decreased as the applied voltage increased, and the desalination performance improved. However, when the voltage exceeded 1.2 V, the effluent conductivity presented an upward trend, and desalination performance decreased. This was probably due to electrode polarization and water splitting occurring at higher applied voltages (>1.23 V) with significant Faraday side reactions. Therefore, the optimal voltage for PAC-9 composite for FCDI was determined to be 1.2 V.

3.4. Long-term operation

The stability performance of electrode materials is critical to the long-term desalination operation of FCDI systems. To investigate the stability of desalination based on PAC composite as flowing electrodes for FCDI, the PAC-9 composite with the best electrochemical performance was used to prepare the flowing electrode with ultrapure water as the electrolyte, and long-term desalination experiments in SC mode were carried out at the feed concentration of 35 g/L NaCl for 12 h running time. Fig. 7a displays the conductivity variation of feed water at 1.2 V applied voltage, and it is obvious that the conductivity shows a nearly linear decreasing trend. Fig. 7b shows the variations of SRE and ASRR within each hour. In the initial period of the long-term operation, the SRE and ASRR both underwent a noticeable drop, which could be explained by the variation of electrical current across the FCDI cell under the long-term desalting test (Figure S11). After 12 h of desalination, a total of 72 % of SRE was achieved and the ASRR was 0.796 μmol cm^{-2} min^{-1}. The higher NaCl removal efficiency and removal rate of the PAC-9 composite compared to the blank flowing electrode (27 % of SRE with 0.30 μmol cm^{-2} min^{-1} of ASRR) during the long-term tests indicate that the PAC-9 composite has good long-term desalination performance. At the same time, it was observed that the electrical current dropped quickly at the initial stage for the PAC-9 composite, but then showed a rise, which is due to the increase of electrolyte concentration in the flow-electrode chamber and the decrease of resistance with the progress of the reaction, and the final decrease in the electrical current is possibly attributed to the increase of resistance in the middle chamber caused by the gradual removal of NaCl in the feed water (Figure S11). It is noteworthy that the SRE within each hour also shows a rising trend with the increase of running time, demonstrating that the PAC-9 composite in SC mode for FCDI technology has a stable pseudo-infinite desalination capacity. In addition, considering that the main degradation product of PANI is benzoquinone, the UV–Vis spectroscopy analysis was performed on the samples of treated water and flowing electrode after a long-term experiment to check whether the PAC composite has undergone unstable degradation. As exhibited in the Figure S12, no significant benzoquinone absorption peak appeared at 240 nm, indicating that AC inhibited the degradation of PANI, and the PAC composite material has a good stability to achieve long-term desalination.

4. Conclusions

The development of more efficient flow-electrode materials is crucial to improving the FCDI performance for salt removal. In this study, the PAC composites were successfully fabricated by the in-situ polymerization of PANI on AC, and then were explored as flowing electrodes of FCDI under the SC operation mode. By comparing the physicochemical properties between the PAC composites, pristine/blank AC and PANI, it was found that the unique hybrid structure of the composites and the excellent charge transfer ability of polyaniline are favorable to promoting the migration and diffusion of ions to improve the desalination performance. The AC provides a large surface for the loading of the polyaniline, and the PANI layer structure establishes a good electron

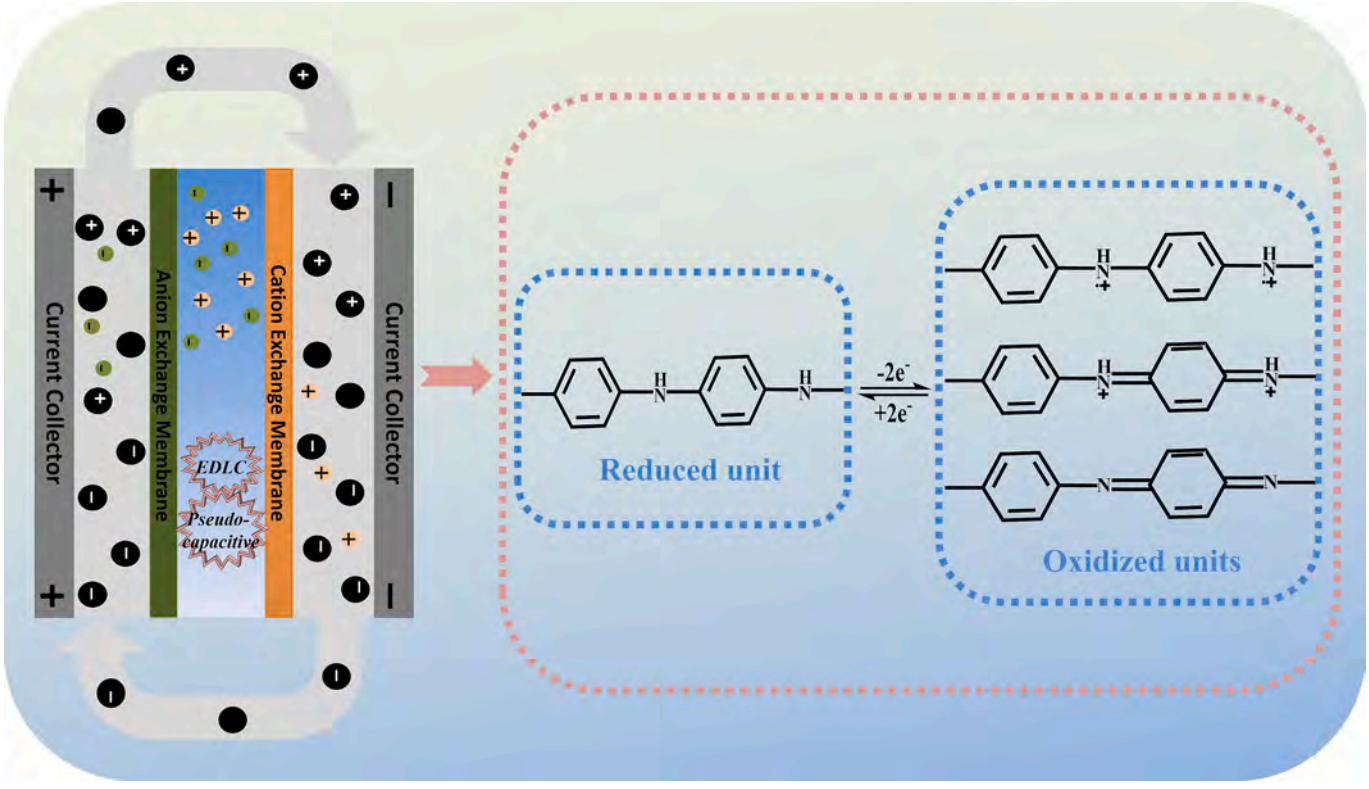

Fig. 6. The mechanistic illustration of water desalination with PAC composite as the flowing electrode.

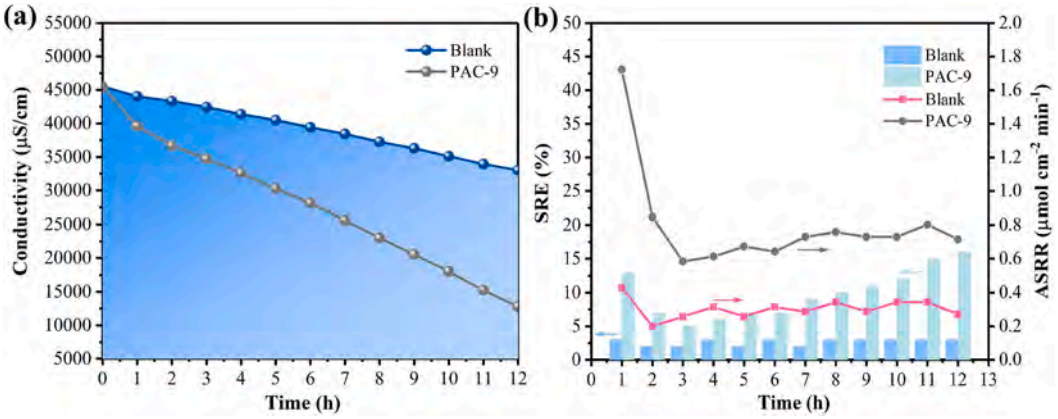

Fig. 7. (a) Change of effluent conductivity in the long-term desalting test; (b) Variations of the ASRR and SRE within each hour.

conduction network. It is more important that the significant capacitance increase of PAC composite is mainly due to the pseudocapacitance from the redox of PANI, thus generating the synergistic effect of EDLC and pseudocapacitance to achieve an excellent desalination performance. Moreover, optimization of the desalination performance can be achieved by adjustment of the load of polyaniline. At a constant voltage of 1.2 V and a feed water of 2 g/L NaCl, the PAC-9 composite exhibited a high desalination efficiency of 94.3 % in 60 min, which was 52.7 % higher than that of AC. Furthermore, during the long-term tests, the PANI degradation products were not detected in the aqueous solution, indicating that the PAC composite is a promising active material.

CRediT authorship contribution statement

Kunyue Luo: Writing – original draft, Investigation, Formal analysis. **Tong Hu:** Writing – review & editing, Methodology, Formal analysis. **Wenle Xing:** Writing – review & editing, Methodology. **Guangming Zeng:** Writing – review & editing, Funding, Supervision. **Wangwang Tang:** Writing – review & editing, Funding, Supervision.

Declaration of competing interest

The authors declare that they have no known competing financial interests or personal relationships that could have appeared to influence the work reported in this paper.

Data availability

Data will be made available on request.

Acknowledgements

This study was financially supported by the National Natural Science Foundation of China (U20A20323, 22276048), the Research and Development Plan of Key Areas in Hunan Province (2022SK2066), the Scientific Research Project of Hunan Provincial Education Department (20K032), and the Natural Science Foundation of Hunan Province (2021JJ30125, 2023JJ40234).

Appendix A. Supplementary data

Supplementary data to this article can be found online at https://doi.org/10.1016/j.cej.2023.148454.

References

[1] V.G. Gude, Desalination and sustainability - An appraisal and current perspective, Water Res. 89 (2016) 87–106.
[2] L. Xu, S. Peng, Y. Mao, Y. Zong, X. Zhang, D. Wu, Enhancing brackish water desalination using magnetic flow-electrode capacitive deionization, Water Res. 216 (2022) 118290.
[3] T. Yu, H. Chen, T. Hu, J. Feng, W. Xing, L. Tang, W. Tang, Recent advances in the applications of encapsulated transition-metal nanoparticles in advanced oxidation processes for degradation of organic pollutants: a critical review, Appl. Catal. b: Environ. 342 (2024) 123401.
[4] J. Du, T.D. Waite, P.M. Biesheuvel, W. Tang, Recent advances and prospects in electrochemical coupling technologies for metal recovery from water, J. Hazard. Mater. 442 (2023) 130023.
[5] C. Zhang, J. Ma, L. Wu, J. Sun, L. Wang, T. Li, T.D. Waite, Flow electrode capacitive deionization (fcdi): recent developments, environmental applications, and future perspectives, Environ. Sci. Tech. 55 (2021) 4243–4267.
[6] E. Menachem, A.P. William, The future of seawater desalination: energy, technology, and the environment, Science 333 (2011) 6043.
[7] J. Du, T.D. Waite, J. Feng, Y. Lei, W. Tang, Coupled electrochemical methods for nitrogen and phosphorus recovery from wastewater: a review, Environ. Chem. Lett. 21 (2023) 885–909.
[8] A. Alkhudhiri, N. Darwish, N. Hilal, Membrane distillation: a comprehensive review, Desalination 287 (2012) 2–18.
[9] A. Subramani, J.G. Jacangelo, Emerging desalination technologies for water treatment: a critical review, Water Res. 75 (2015) 164–187.
[10] A. Subramani, M. Badruzzaman, J. Oppenheimer, J.G. Jacangelo, Energy minimization strategies and renewable energy utilization for desalination: a review, Water Res. 45 (2011) 1907–1920.
[11] M. Qin, A. Deshmukh, R. Epsztein, S.K. Patel, O.M. Owoseni, W.S. Walker, M. Elimelech, Comparison of energy consumption in desalination by capacitive deionization and reverse osmosis, Desalination 455 (2019) 100–114.
[12] L. Shi, J. Huang, G. Zeng, L. Zhu, Y. Gu, Y. Shi, K. Yi, X. Li, Roles of surfactants in pressure-driven membrane separation processes: a review, Environ. Sci. Pollut. Res. 26 (2019) 30731–30754.
[13] S. Porada, R. Zhao, A. van der Wal, V. Presser, P.M. Biesheuvel, Review on the science and technology of water desalination by capacitive deionization, Prog. Mater Sci. 58 (2013) 1388–1442.
[14] C. Zhang, D. He, J. Ma, W. Tang, T.D. Waite, Faradaic reactions in capacitive deionization (CDI) - problems and possibilities: a review, Water Res. 128 (2018) 314–330.
[15] Z. Lu, Q. Yang, T. Hu, J. Wang, W. Tang, $Fe^{II}Al^{III}$ layered double hydroxide modified carbon-felt cathode for efficient electrochemical reduction of bromate, Chem. Eng. J. 446 (2022) 137356.
[16] M.E. Suss, S. Porada, X. Sun, P.M. Biesheuvel, J. Yoon, V. Presser, Water desalination via capacitive deionization: what is it and what can we expect from it? Energ. Environ. Sci. 8 (2015) 2296–2319.
[17] J. Du, W. Xing, J. Yu, J. Feng, L. Tang, W. Tang, Synergistic effect of intercalation and EDLC electrosorption of 2D/3D interconnected architectures to boost capacitive deionization for water desalination via MoSe2/mesoporous carbon hollow spheres, Water Res. 235 (2023) 119831.
[18] P. Nativ, Y. Badash, Y. Gendel, New insights into the mechanism of flow-electrode capacitive deionization, Electrochem. Commun. 76 (2017) 24–28.
[19] S.-I. Jeon, H.-R. Park, J.-G. Yeo, S. Yang, C.H. Cho, M.H. Han, D.K. Kim, Desalination via a new membrane capacitive deionization process utilizing flow-electrodes, Energ. Environ. Sci. 6 (2013) 1471.
[20] F. Yang, Y. He, L. Rosentsvit, M.E. Suss, X. Zhang, T. Gao, P. Liang, Flow-electrode capacitive deionization: a review and new perspectives, Water Res. 200 (2021) 117222.
[21] A. Feng, J. Feng, W. Xing, K. Jiang, W. Tang, Versatile applications of electrochemical flow-through systems in water treatment processes, Chem. Eng. J. 473 (2023) 145400.
[22] Y. Cho, C.Y. Yoo, S.W. Lee, H. Yoon, K.S. Lee, S. Yang, D.K. Kim, Flow-electrode capacitive deionization with highly enhanced salt removal performance utilizing high-aspect ratio functionalized carbon nanotubes, Water Res. 151 (2019) 252–259.

[23] K.Y. Choo, C.Y. Yoo, M.H. Han, D.K. Kim, Electrochemical analysis of slurry electrodes for flow-electrode capacitive deionization, J. Electroanal. Chem. 806 (2017) 50–60.
[24] L. Zou, L. Li, H. Song, G. Morris, Using mesoporous carbon electrodes for brackish water desalination, Water Res. 42 (2008) 2340–2348.
[25] K. Tang, S. Yiacoumi, Y. Li, C. Tsouris, Enhanced water desalination by increasing the electroconductivity of carbon powders for high-performance flow-electrode capacitive deionization, ACS Sustain. Chem. Eng. 7 (2018) 1085–1094.
[26] J. Ma, C. Zhang, F. Yang, X. Zhang, M.E. Suss, X. Huang, P. Liang, Carbon black flow electrode enhanced electrochemical desalination using single-cycle operation, Environ. Sci. Tech. 54 (2020) 1177–1185.
[27] K.B. Hatzell, M.C. Hatzell, K.M. Cook, M. Boota, G.M. Housel, A. McBride, E. C. Kumbur, Y. Gogotsi, Effect of oxidation of carbon material on suspension electrodes for flow electrode capacitive deionization, Environ. Sci. Tech. 49 (2015) 3040–3047.
[28] K. Luo, M. Chen, W. Xing, M. Duan, J. Du, G. Zeng, W. Tang, Significantly enhanced desalination performance of flow-electrode capacitive deionization via cathodic iodide redox couple and its great potential in treatment of iodide-containing saline wastewater, Chem. Eng. J. 421 (2021) 129905.
[29] H.-R. Park, J. Choi, S. Yang, S.J. Kwak, S.-I. Jeon, M.H. Han, D.K. Kim, Surface-modified spherical activated carbon for high carbon loading and its desalting performance in flow-electrode capacitive deionization, RSC Adv. 6 (2016) 69720–69727.
[30] G.J. Doornbusch, J.E. Dykstra, P.M. Biesheuvel, M.E. Suss, Fluidized bed electrodes with high carbon loading for water desalination by capacitive deionization, J. Mater. Chem. A 4 (2016) 3642–3647.
[31] J. Wu, X. Xuan, S. Zhang, Z. Li, H. Li, B. Zhao, H. Ye, Z. Xiao, X. Zhao, X. Xu, X. Liu, J. You, Y. Yamauchi, N, P-doped carbon nanorings for high-performance capacitive deionization, Chem. Eng. J. 473 (2023) 145421.
[32] X. Liu, X. Xu, X. Xuan, W. Xia, G. Feng, S. Zhang, Z.-G. Wu, B. Zhong, X. Guo, K. Xie, Y. Yamauchi, Unlocking enhanced capacitive deionization of NaTi2(PO4)3/carbon materials by the yolk-shell design, J. Am. Chem. Soc. 145 (2023) 9242–9253.
[33] Z. Xing, X. Xuan, H. Hu, M. Li, H. Gao, A. Alowasheeir, D. Jiang, L. Zhu, Z. Li, Y. Kang, J. Zhang, X. Yi, Y. Yamauchi, X. Xu, Particle size optimization of metal–organic frameworks for superior capacitive deionization in oxygenated saline water, Chem. Commun. 59 (2023) 4515–4518.
[34] X. Xu, M. Eguchi, Y. Asakura, L. Pan, Y. Yamauchi, Metal–organic framework derivatives for promoted capacitive deionization of oxygenated saline water, Energ. Environ. Sci. 16 (2023) 1815–1820.
[35] X. Li, W. Xing, T. Hu, K. Luo, J. Wang, W. Tang, Recent advances in transition-metal phosphide electrocatalysts: synthetic approach, improvement strategies and environmental applications, Coord. Chem. Rev. 473 (2022) 214811.
[36] T. Hu, L. Tang, H. Feng, J. Zhang, X. Li, Y. Zuo, Z. Lu, W. Tang, Metal-organic frameworks (MOFs) and their derivatives as emerging catalysts for electro-Fenton process in water purification, Coord. Chem. Rev. 451 (2022) 214277.
[37] F. Yu, L. Wang, Y. Wang, X. Shen, Y. Cheng, J. Ma, Faradaic reactions in capacitive deionization for desalination and ion separation, J. Mater. Chem. A 7 (2019) 15999–16027.
[38] M.E. Suss, V. Presser, Water desalination with energy storage electrode materials, Joule 2 (2018) 10–15.
[39] W. Xing, K. Luo, J. Liang, C. Su, W. Tang, Urchin-like core–shell tungsten oxide@carbon composite electrode for highly efficient and stable water desalination via hybrid capacitive deionization (HCDI), Chem. Eng. J. 477 (2023) 147268.
[40] F. Meng, Z. Ding, X. Xu, Y. Liu, T. Lu, L. Pan, Metal organic framework-derived nitrogen-doped porous carbon sustained Prussian blue analogues for efficient and fast hybrid capacitive deionization, Sep. Purif. Technol. 317 (2023) 123899.
[41] L. Xu, Z. Ding, Y. Chen, X. Xu, Y. Liu, J. Li, T. Lu, L. Pan, Carbon nanotube bridged nickel hexacyanoferrate architecture for high-performance hybrid capacitive deionization, J. Colloid Interface Sci. 630 (2023) 372–381.
[42] Y. Zuo, J. Feng, T. Soyol-Erdene, Z. Wei, T. Hu, Y. Zhang, W. Tang, Recent advances in wood-derived monolithic carbon materials: synthesis approaches, modification methods and environmental applications, Chem. Eng. J. 463 (2023) 142332.
[43] G.A. Snook, P. Kao, A.S. Best, Conducting-polymer-based supercapacitor devices and electrodes, J. Power Sources 196 (2011) 1–12.
[44] W.-M. Chang, C.-C. Wang, C.-Y. Chen, Plasma-induced polyaniline grafted on carbon nanotube-embedded carbon nanofibers for high-performance supercapacitors, Electrochim. Acta 212 (2016) 130–140.
[45] K.B. Hatzell, M. Beidaghi, J.W. Campos, C.R. Dennison, E.C. Kumbur, Y. Gogotsi, A high performance pseudocapacitive suspension electrode for the electrochemical flow capacitor, Electrochim. Acta 111 (2013) 888–897.
[46] Z. Gao, W. Yang, J. Wang, H. Yan, Y. Yao, J. Ma, B. Wang, M. Zhang, L. Liu, Electrochemical synthesis of layer-by-layer reduced graphene oxide sheets/polyaniline nanofibers composite and its electrochemical performance, Electrochim. Acta 91 (2013) 185–194.
[47] W. Shi, X. Liu, T. Deng, S. Huang, M. Ding, X. Miao, C. Zhu, Y. Zhu, W. Liu, F. Wu, C. Gao, S.W. Yang, H.Y. Yang, J. Shen, X. Cao, Enabling superior sodium capture for efficient water desalination by a tubular polyaniline decorated with prussian blue nanocrystals, Adv. Mater. 32 (2020) e1907404.
[48] Q. Meng, K. Cai, Y. Chen, L. Chen, Research progress on conducting polymer based supercapacitor electrode materials, Nano Energy 36 (2017) 268–285.
[49] Y.G. Wang, H.Q. Li, Y.Y. Xia, Ordered whiskerlike polyaniline grown on the surface of mesoporous carbon and its electrochemical capacitance performance, Adv. Mater. 18 (2006) 2619–2623.
[50] Y. Zhou, Z.-Y. Qin, L. Li, Y. Zhang, Y.-L. Wei, L.-F. Wang, M.-F. Zhu, Polyaniline/multi-walled carbon nanotube composites with core–shell structures as supercapacitor electrode materials, Electrochim. Acta 55 (2010) 3904–3908.
[51] G. Jiang, J. Cai, M. Krishnamoorthy, R.A. Senthil, Y. Sun, X. Li, J. Pan, Controlling morphologies and structures of PANI@Carbon with superior rate performance for supercapacitors, ACS Appl. Energy Mater. 5 (2022) 4138–4148.
[52] P. Singh, K. Pal, Activated carbon-Polyaniline composite active material slurry electrode for high capacitance, improved rheological performance electrochemical flow capacitor, Electrochim. Acta 354 (2020) 136719.
[53] Z. Wang, L. Jiang, Y. Wei, C. Zong, In-situ polymerization to prepare reduced graphene oxide/polyaniline composites for high performance supercapacitors, J. Energy Storage 32 (2020) 101742.
[54] Y. Sun, D. Shao, C. Chen, S. Yang, X. Wang, Highly efficient enrichment of radionuclides on graphene oxide-supported polyaniline, Environ. Sci. Tech. 47 (2013) 9904–9910.
[55] L. Lyu, H. Chai, K.-D. Seong, C. Lee, J. Kang, W. Zhang, Y. Piao, Yeast-derived N-doped carbon microsphere/polyaniline composites as high performance pseudocapacitive electrodes, Electrochim. Acta 291 (2018) 256–266.
[56] J. Wang, J. Feng, T. Soyol-Erdene, Z. Wei, W. Tang, Electrodeposited NiCoP on nickel foam as a self-supported cathode for highly selective electrochemical reduction of nitrate to ammonia, Sep. Purif. Technol. 320 (2023) 124155.
[57] J. Li, D. Xiao, Y. Ren, H. Liu, Z. Chen, J. Xiao, Bridging of adjacent graphene/polyaniline layers with polyaniline nanofibers for supercapacitor electrode materials, Electrochim. Acta 300 (2019) 193–201.
[58] F. Gao, X. Li, W. Shi, Z. Wang, Highly selective recovery of phosphorus from wastewater via capacitive deionization enabled by ferrocene-polyaniline-functionalized carbon nanotube electrodes, ACS Appl. Mater. Inter. 14 (2022) 31962–31972.
[59] J. Zhao, Y. Li, X. Chen, H. Zhang, C. Song, Z. Liu, K. Zhu, K. Cheng, K. Ye, J. Yan, D. Cao, G. Wang, X. Zhang, Polyaniline-modified porous carbon tube bundles composite for high-performance asymmetric supercapacitors, Electrochim. Acta 292 (2018) 458–467.
[60] J. Zhang, D. Wang, F. Zhao, J. Feng, H. Feng, J. Luo, W. Tang, Ferrate modified carbon felt as excellent heterogeneous electro-Fenton cathode for chloramphenicol degradation, Water Res. 227 (2022) 119324.
[61] N. Gavrilov, I.A. Pašti, M. Vujković, J. Travas-Sejdic, G. Ćirić-Marjanović, S. V. Mentus, High-performance charge storage by N-containing nanostructured carbon derived from polyaniline, Carbon 50 (2012) 3915–3927.
[62] K.S.G.C. Oliveira, K.M. Barcelos, J.J. Lado, J. Palma, L.A.M. Ruotolo, Improving the electrochemical desalination performance of chloride-doped polyaniline activated carbon electrode by tuning the synthesis method, Chem. Eng. J. 457 (2023) 141059.
[63] K. Zhang, L.L. Zhang, X.S. Zhao, J. Wu, Graphene/polyaniline nanofiber composites as supercapacitor electrodes, Chem. Mater. 22 (2010) 1392–1401.
[64] B. Li, Q. Cao, Y. Liu, Y. Sun, X. Ma, X. Duan, C. Chen, Y. Wang, Polyaniline-decorated porous carbons with engineered meso/macrochannels for high performance capacitive deionization, J. Mater. Chem. A 10 (2022) 24905–24914.
[65] X. Chen, P. Liu, C. Liu, G. Liu, J. Wei, J. Xu, Q. Jiang, X. Liu, F. Jiang, Microstructure control for high-capacitance polyaniline, Electrochim. Acta 391 (2021) 138977.
[66] J.W. Jeon, J. O'Neal, L. Shao, J.L. Lutkenhaus, Charge storage in polymer acid-doped polyaniline-based layer-by-layer electrodes, ACS Appl. Mater. Interfaces 5 (2013) 10127–10136.
[67] W. Jin, J. Feng, W. Xing, W. Tang, Significantly enhanced electrocatalytic reduction of chloramphenicol from water mediated by Fe-F-N co-doped carbon materials, ACS ES&T Water 3 (2023) 1385–1394.
[68] C.O. Baker, X. Huang, W. Nelson, R.B. Kaner, Polyaniline nanofibers: broadening applications for conducting polymers, Chem. Soc. Rev. 46 (2017) 1510–1525.
[69] W. Tang, J. Liang, D. He, J. Gong, L. Tang, Z. Liu, D. Wang, G. Zeng, Various cell architectures of capacitive deionization: recent advances and future trends, Water Res. 150 (2019) 225–251.